MgB_2 nonlinear properties investigated under localized high rf magnetic field excitation

Tamin Tai,[1,2] B. G. Ghamsari,[2] T. Tan,[3] C. G. Zhuang,[3] X. X. Xi,[3] and Steven M. Anlage[1,2]

[1]*Department of Electrical and Computer Engineering, University of Maryland, College Park, Maryland 20742-3285, USA*
[2]*Department of Physics, Center for Nanophysics and Advanced Materials, University of Maryland, College Park, Maryland 20742-4111, USA*
[3]*Physics Department, Temple University, Philadelphia, Pennsylvania 19122, USA*

(Received 29 December 2011; published 10 December 2012)

The high transition temperature and low surface resistance of MgB_2 attracts interest in its potential application in superconducting radio frequency accelerating cavities. However, compared to traditional Nb cavities, the viability of MgB_2 at high rf fields is still open to question. Our approach is to study the nonlinear electrodynamics of the material under localized rf magnetic fields. Because of the presence of the small superconducting gap in the π band, the nonlinear response of MgB_2 at low temperature is potentially complicated compared to a single-gap s-wave superconductor such as Nb. Understanding the mechanisms of nonlinearity coming from the two-band structure of MgB_2, as well as extrinsic sources of nonlinearity, is an urgent requirement. A localized and strong rf magnetic field, created by a magnetic write head, is integrated into our nonlinear-Meissner-effect scanning microwave microscope [T. Tai *et al.*, IEEE Trans. Appl. Supercond. **21**, 2615 (2011)]. MgB_2 films with thickness 50 nm, fabricated by a hybrid physical-chemical vapor deposition technique on dielectric substrates, are measured at a fixed location and show a strongly temperature-dependent third harmonic response. We propose that several possible mechanisms are responsible for this nonlinear response.

DOI: 10.1103/PhysRevSTAB.15.122002 PACS numbers: 74.70.Ad, 74.25.Uv, 74.78.−w, 07.79.−v

I. INTRODUCTION

The discovery of superconductivity in MgB_2 in January 2001 [1] ignited enthusiasm and interest in exploring its material properties. Several remarkable features, for example a high transition temperature ($T_c \sim 40$ K), a high critical field, and a low rf surface resistance below T_c, show great potential in several applications such as superconducting wires and magnets. The success of making high quality epitaxial MgB_2 thin films provides another promising application as an alternative material coating on superconducting radio frequency (SRF) cavities [2]. Over the past decade, the accelerating gradient has achieved 59 MeV/m in the fine-grain niobium (Nb) single cell cavity [3]. In order to go further, new high T_c materials with low rf resistance are required for interior coating of bulk Nb cavities. High quality MgB_2 thin films may satisfy the demands for SRF coating materials because such films can avoid the weak link nonlinearity between grains, and lead to the possibility of making high-Q cavities [4].

However, there still exist mechanisms that produce nonideal behavior at low temperatures under high rf magnetic fields, such as vortex nucleation and motion in the film [5]. In addition, due to the presence of the π band and σ band, the intrinsic nonlinear response of MgB_2 at low temperature is large compared to single-gap s-wave superconductors [6,7]. Finally, it has been proposed that MgB_2 has 6 nodes in its energy gap [8]. The intermodulation distortion (IMD) measurements show a strong enhancement at low temperature (T) as $P_{\mathrm{IMD}}(T) \sim 1/T^2$ [9], similar to the characteristics of the d-wave nodal $YBa_2Cu_3O_{7-\delta}$ (YBCO) superconductor [10]. Note that the nodal nonlinear Meissner effect has only been measured by means of nonlinear microwave techniques up to this point. If MgB_2 is a nodal superconductor, the coating of MgB_2 on SRF cavities will limit the high-field screening response at low temperature and therefore degrade the performance of the SRF cavities. Based on the above concerns, the study of MgB_2 microwave nonlinear response in the high frequency region (usually several GHz in SRF applications) can reveal the dissipative and nondissipative nonlinear mechanisms and perhaps enable application of MgB_2 films as cavity coatings.

In our experiment the localized harmonic response of superconductors is excited by a magnetic write head probe extracted from a commercial magnetic hard drive [11]. Based on the gap geometry of the magnetic write head probe, submicron resolution is expected. We present our observation of the nonlinear response of high quality MgB_2 films below T_c. These films were grown on (0001) sapphire substrates by the hybrid physical-chemical vapor deposition technique (HPCVD). A (0001)-oriented MgB_2 film with $(10\bar{1}0)$ in-plane epitaxial structure was determined by θ-2θ and ϕ scans in x-ray diffraction, respectively.

A detailed description of the growth technique and their structural analysis has been reported before [12].

It should be noted that the SRF cavities function at very low temperature and in rf magnetic fields of varying strength, depending on location in the cavity. However, our microscope functions at temperatures down to 5 K, and with a localized high rf magnetic field. Therefore our microscope is best suited for finding the localized electromagnetic response of the surface. We expect to find electromagnetic contrast due to surface defects on the materials of the cavities. In this paper, we report the MgB_2 experimental nonlinearity data from localized areas. These data will be interpreted as a combination of several nonlinear mechanisms including intrinsic nonlinear responses [7,8] and vortex nonlinearity [5].

II. EXPERIMENTAL SETUP

The experimental setup for amplitude and phase measurements of the superconductor harmonic response is shown in Fig. 1. An excited wave (fundamental signal) at frequency f comes from the vector network analyzer (VNA) and is low-pass filtered to eliminate higher harmonics of the source signal. This fundamental tone is sent to the magnetic write head probe to generate a localized rf magnetic field on the superconductor sample. Two insets in Fig. 1 show close-up views of our magnetic write head probe on superconducting samples. Because of the intense nature of this field, the superconductor responds by generating screening currents at both the fundamental frequency and at harmonics of this frequency. The generated and coupled harmonic signal is high-pass filtered to remove the fundamental signal V_f and an unratioed measurement of V_{3f} is performed on port 2 of the VNA. In order to get a phase-sensitive measurement of the 3rd harmonic signal coming from the superconducting sample, a harmonic generation circuit is connected to provide a reference 3rd harmonic signal, and the relative phase difference between the main circuit and reference circuit is measured. Further details about this phase-sensitive measurement technique can be found in Ref. [13]. In this way we measure the complex third harmonic voltage of $V_{3f}^{\text{sample}}(T)$ or the corresponding scalar power $P_{3f}^{\text{sample}}(T)$. The lowest noise floor in our VNA is -130 dBm for the unratioed power measurement. A ratioed measurement of the complex $V_{3f}^{\text{sample}}(T)/V_{3f}^{\text{ref}}$ is also performed at the same time. An alternative method to lower the noise floor is to remove the VNA and use a stable synthesizer on port 1 and a phase-locked spectrum analyzer on port 2. The noise floor of our spectrum analyzer (model number: ESA-E E4407B) is -145 dBm. In this paper we only discuss the unratioed measurements of $P_{3f}^{\text{sample}}(T)$ and qualitatively discuss the mechanisms of third harmonic response of the MgB_2 film.

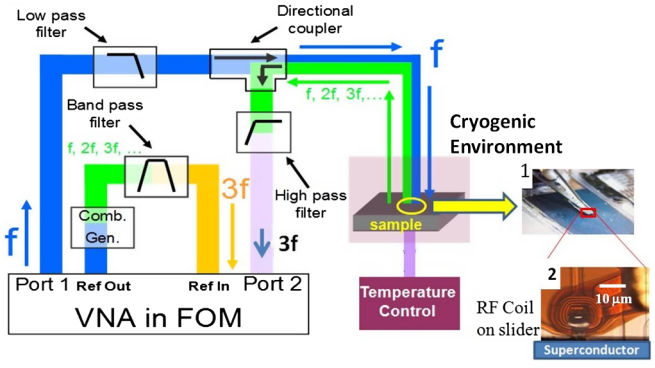

FIG. 1. Setup of phase-sensitive harmonic measurement in nonlinear microwave microscopy. The frequency offset mode (FOM) of a vector network analyzer (VNA: model PNA-X N5242A) is used in this measurement. Inset 1 shows the magnetic write head probe assembly on top of a superconducting thin film and inset 2 is a picture of the rf microcoil of the probe above the sample.

III. THIRD ORDER NONLINEAR MEASUREMENT RESULTS

The measurement of the 3rd order harmonic power (P_{3f}) is performed near the center of several epitaxial MgB_2 films with the same thickness, 50 nm. The T_c of these samples are around 32–35 K measured by the four point resistance method. These samples are all grown on sapphire substrates under the same deposition conditions by the HPCVD method. These samples can be grouped into two classes: Group A are the samples which are not well isolated from the ambient environment after growth. Group B are the samples which are kept in desiccated conditions immediately after deposition. At least two samples are measured from each group to examine their rf microwave properties. Figure 2 shows a representative temperature-dependent $P_{3f}(T)$ curve for the sample from group A at the excited frequency 5.33 GHz and excited power $+14$ dBm. Above 40 K a very small signal begins to

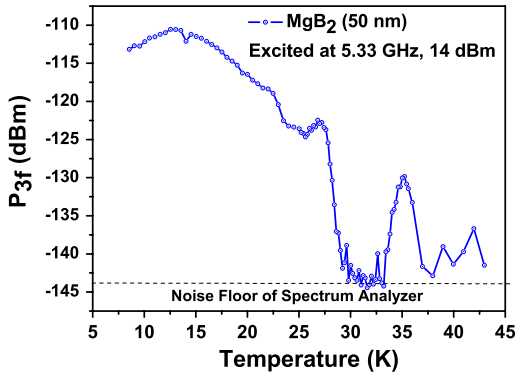

FIG. 2. Temperature dependence of 3rd harmonic power P_{3f} from a 50 nm thick MgB_2 of group A measured with an excited frequency of 5.33 GHz at $+14$ dBm.

arise above the noise floor of the spectrum analyzer. This P_{3f} is from the magnetic write head probe itself. We have measured the P_{3f} of the magnetic probe when it is placed on the surface of a bare sapphire substrate and in general this probe nonlinearity is negligible at excited powers under +14 dBm. Although excited powers above +14 dBm excites stronger nonlinearity from the probe, this nonlinearity is almost temperature independent in the helium cooling temperature range. Therefore probe nonlinearity, if it is present, can be treated as a constant background signal above the noise floor of the spectrum analyzer/VNA. The mechanism of probe nonlinearity is the hysteretic behavior of the yoke material, and has been discussed previously [11].

From Fig. 2, a clear $P_{3f}(T)$ peak centered at 35 K shows up above the noise floor. This peak arises from the modulation of the superconducting order parameter near T_c due to the enhanced sensitivity of superconducting properties as the superfluid density decreases to near-zero levels. This peak at T_c is also phenomenologically predicted by Ginzburg-Landau theory, and is discussed further below.

We also note the onset of a temperature-dependent P_{3f} nonlinearity below 29 K, followed by a peak near 27 K, and then a gradually increasing P_{3f} down to 12.5 K. Finally, the P_{3f} decreases below 12.5 K.

Measurements of the dependence of P_{3f} on P_f are shown in Fig. 3 for the 50 nm thick MgB_2 film (group A) at some selected temperatures. In the normal state of MgB_2 ($T = 42$ K), the measured nonlinearity comes from the probe itself and shows a slope steeper than 3 at high excited power above +15 dBm. Near T_c, the slope is 2.74, close to the value of 3 as predicted for the intrinsic nonlinear response [14]. Based in part on this evidence, we believe that in the high temperature region close to T_c, most of the P_{3f} comes from the intrinsic nonlinear mechanism related to the modulation of the order parameter near T_c. In the intermediate and low temperature regime, the slopes of P_{3f} vs P_f are between 1–2. This value is similar to that predicted by many phenomenological models (between 1–2) for YBCO films at low temperature [10,15], implying that several possible nonlinear mechanisms are involved at low temperature for MgB_2 films. It should be noted that the low temperature nonlinearity can be easily excited at low power. Figure 3 shows the P_{3f}-P_f slope evolution from an intrinsic nonlinear region around T_c to a regime with different behavior at lower temperature.

The representative curve of $P_{3f}(T)$ from a sample of group B is shown in Fig. 4. Compared with the measurement of $P_{3f}(T)$ from the sample of group A, as shown in Fig. 2, many temperature-dependent nonlinear features are consistent and reproducible. From Fig. 4, the first peak at 32 K represents the first T_c of this sample. A second peak at 22.5 K, similar to that at 27 K (Fig. 2) is distinctly visible in Fig. 4. The only difference is a second deep dip around

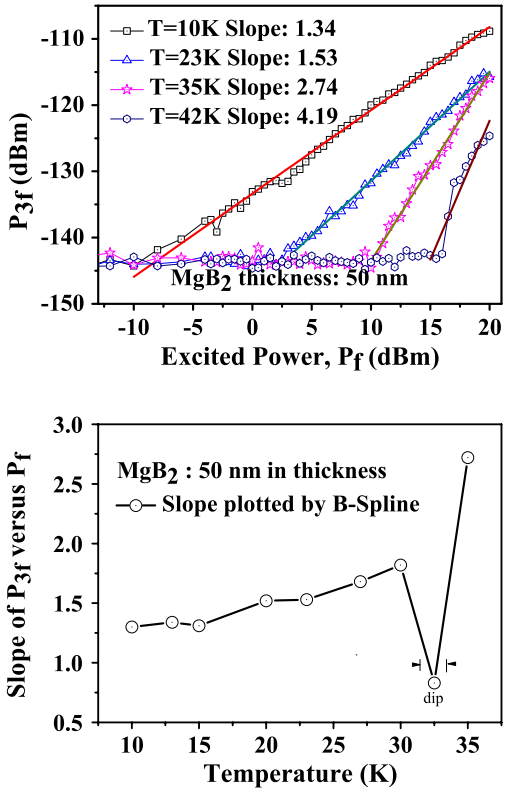

FIG. 3. (top frame) Power dependence of P_{3f} on P_f for the 50 nm thick MgB_2 film of group A. (bottom frame) Fitted slope at selected temperatures for the film of group A. The marked dip describes an almost nonlinearity-free region from the MgB_2 sample and its small slope is likely due to the probe nonlinearity.

20 K for the sample from group B, versus a shallow dip at 25 K for the sample from group A in the $P_{3f}(T)$ measurement. The position of the dip and its depth also change with the excited power. This sharp dip indicates the near cancellation of all nonlinear mechanisms at this temperature. For both groups of samples, the nonlinearity gradually increases with reduced temperature below the second dip,

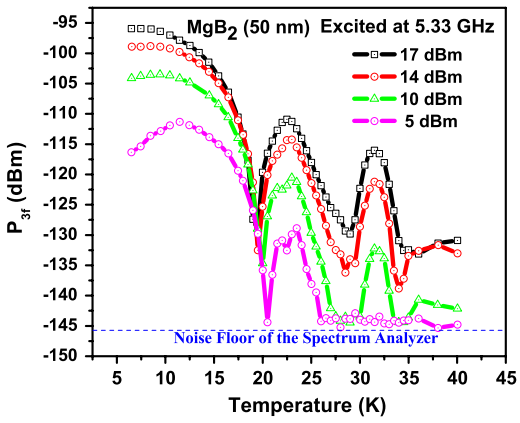

FIG. 4. Temperature dependence of 3rd harmonic power P_{3f} from a 50 nm thick MgB_2 of group B measured with an excited frequency of 5.33 GHz at different excited powers.

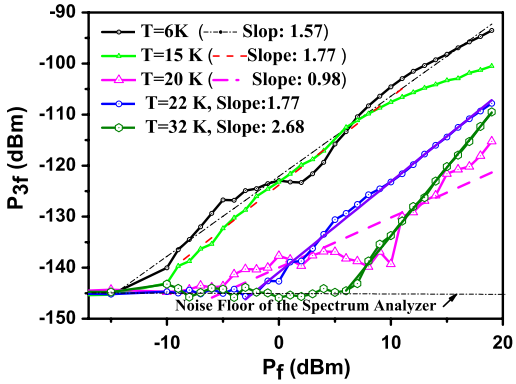

FIG. 5. Power dependence of P_{3f} on P_f for the 50 nm thick MgB_2 film of group B.

followed by a saturation and finally a decrease at temperatures below 10 K, at least for lower excitation power.

Figure 5 shows the dependence of P_{3f} on P_f for the sample from group B. At T_c (32 K), the slope of the power dependence is almost 3. Below T_c, the slope drops to a value between 1–2, the same as many published results on MgB_2 [16,17], excluding the points near 20 K at which the slope drops below one. This point (the second dip) shows very small nonlinearity from the superconductor below 10 dBm excitation. For high excitation power (above 10 dBm), the majority of the nonlinearity signal comes from the probe itself. In addition, at some temperatures (20, 15, and 6 K), the power dependence curve shows several changes of slope. This implies that the nonlinear behavior is more complex at intermediate and low temperatures. Therefore based on the similar nonlinear behavior of many measured MgB_2 samples, we next discuss several possible mechanisms that may account for the basic common features of our experimental data.

IV. INTRINSIC NONLINEARITY OF MgB_2 AROUND T_c

The modulation of superconducting order parameter generates nonlinearity under excitation by an applied field. While the excitation field is much lower than the critical field, nonlinearity will be generated due to the perturbation of the ordered parameter. This phenomenon is generally known as a nonlinear Meissner effect (NLME). When the excitation field approaches the critical field, the mechanism of intrinsic nonlinearity is still similar to the NLME and becomes more significant. For example, around T_c, this nonlinearity comes from the backflow of excited quasiparticles in a current-carrying superconductor, which results in an effective decrease of the superfluid density [7,8,18]. A two-band quasiparticle backflow calculation has been applied to the MgB_2 intrinsic nonlinearity. Based on the work of Dahm and Scalapino [7], the temperature and induced current density dependent superfluid density $n_s(T, J)$ can be written as

$$\frac{n_s(T,J)}{n_s(T,0)} = 1 - \left(\frac{J}{J_{\mathrm{NL}}}\right)^2; \qquad J_{\mathrm{NL}} = \frac{J_{c,\pi}}{\sqrt{b_\pi(T) + b_\sigma(T)\frac{J_{c,\pi}^2}{J_{c,\sigma}^2}}}, \tag{1}$$

where b_σ and b_π are the temperature-dependent nonlinear coefficients for the σ band and π band, respectively, and their values are defined in Ref. [7]. Here $J_{c,\sigma} = 4.87 \times 10^8$ A/cm^2 and $J_{c,\pi} = 3.32 \times 10^8$ A/cm^2 are the pair-breaking current densities for the two bands. For a 50 nm thick MgB_2 thin film, the generated third harmonic power $P_{3f}(T)$ is estimated by substituting J_{NL} into the following equation derived from the assumption of d (thickness) $\ll \lambda$ (penetration depth) [14],

$$P_{3f}(T) = \frac{\omega^2\mu_0^2\lambda^4(T)\Gamma^2(K_{\mathrm{rf}})}{32Z_0d^6J_{\mathrm{NL}}^4(T)} \propto P_f^3;$$
$$\Gamma(K_{\mathrm{rf}}) = I_{\mathrm{tot}}\int\frac{\int K^4(x,y)dx}{(\int K_y dx)^2}dy, \tag{2}$$

where ω is the angular frequency of the incident wave, $\lambda(T)$ is the temperature-dependent magnetic penetration depth, Z_0 is the characteristic impedance of the transmission line in the microscope, I_{tot} is the total current flowing through a cross section right beneath the bottom of the probe, and $\Gamma(K_{\mathrm{rf}})$ is a geometry factor. The value of the geometry factor depends on the distribution of surface current density $[K_{\mathrm{rf}}(x,y)]$ on the superconducting plane. We calculate the surface current from the Karlqvist equation [19], which gives the magnetic field distribution outside the gap in the x-z plane as schematically shown in Fig. 6. Under the treatment of the Karlqvist 2D assumption, the fields are invariant in the y direction along the gap. By only considering the x component of magnetic field (H_x) on the superconducting surface, which is doubled with respect to free space by the boundary condition of the surface, the surface current K_y can be written as

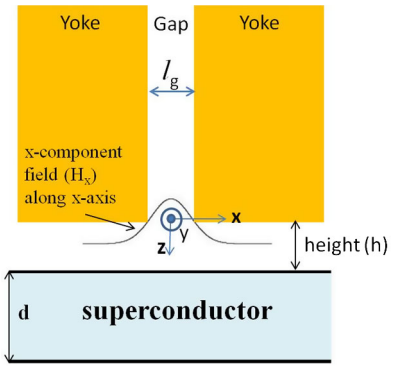

FIG. 6. Schematic illustration of the 2D magnetic write head on the top of the superconductor. The origin is at the bottom of the head centered at the middle of the gap. Gap length (l_g) and film thickness (d) are not to scale.

$$K_y = \frac{2B_g}{\mu_0} \arctan\left[\frac{l_g z}{x^2 + z^2 - (l_g/2)^2}\right], \qquad (3)$$

where B_g is the maximum field strength inside the gap, l_g is the length of the gap, and x, z are distances in the x and z directions with the origin centered in the middle on the bottom of the gap. In reality, the gap is of finite thickness in the y direction as shown in the schematic yoke picture of Fig. 10 with thickness l_y. By assuming that the currents are uniform in the y direction between $y = 0$ and $y = l_y$ and ignoring the return currents, the current distribution geometry factor Γ can be approximated as

$$\Gamma = \frac{l_y \int_{-\ell}^{\ell} K_y^4 dx}{I_{\text{tot}}}; \qquad I_{\text{tot}} = \int_{-\ell}^{\ell} K_y dx, \qquad (4)$$

where ℓ is the distance from the center of maximum current to the node of minimum current as shown in the inset of Fig. 7. In addition, Fig. 7 shows the height (h) dependence of Γ when evaluating K_y at $z = h$. In our calculation, we assume $B_g = 1$ Tesla, $l_g = 100$ nm and probe height $h = 2$ μm above the superconducting surface. Therefore the value of the Γ can be estimated to be 8.3×10^5 A^3/m^2. We note that the probe geometry factor is a strong function of height and can lead to surface fields above the critical field of the superconductor [20].

Finally, the $P_{3f}(T)$ calculated results from (2) for the 50 nm thick film at a 5.33 GHz excited frequency is shown as the solid red line in Fig. 8, assuming the cutoff of $\lambda(T \to T_c)$, $J_{\text{NL}}(T \to T_c)$ and a Gaussian distribution of T_c [14]. This intrinsic response has measurable values

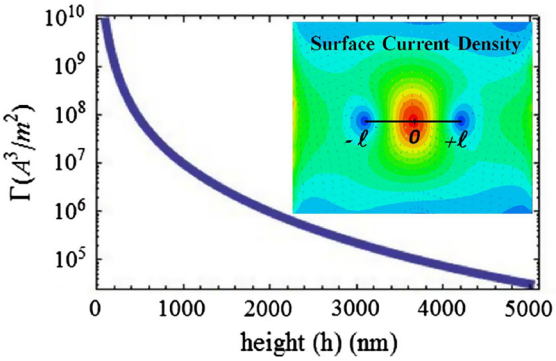

FIG. 7. Calculation of height dependence (h is the $+Z$ direction) of the probe geometry factor $\Gamma(K_{\text{rf}})$ for the longitudinal magnetic write head probe. The black line in the inset shows the integral path of Eq. (4) on the plot of the surface current density simulated by the ANSYS high frequency structure simulator (HFSS) under the assumption that the magnetic writer is 2 μm away from a perfect conductor surface. Red corresponds to large current while blue corresponds to small current. The value of ℓ is on the scale of the outside edge dimension of the magnetic yoke, which is 1.5 μm in the HFSS simulation, and is effectively infinite in the Karlqvist calculation since the return currents are not considered.

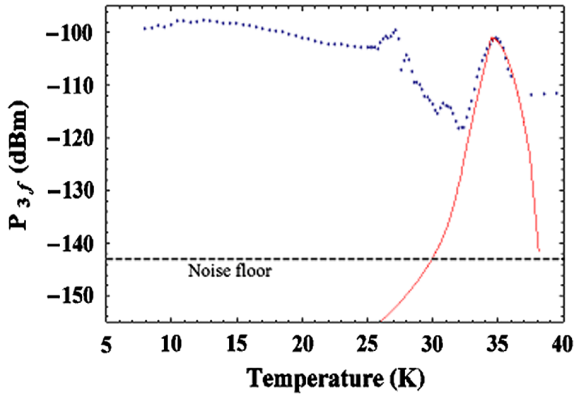

FIG. 8. The blue dots are the MgB_2 $P_{3f}(T)$ data (from group A) at an excitation frequency of 5.33 GHz and excitation power of 18 dBm. The solid red line is the simulated result of the intrinsic nonlinearity from superconducting order parameter modulation near T_c of MgB_2 with thickness 50 nm under the assumption that the magnetic probe provides a field described by a geometry factor $\Gamma = 8.3 \times 10^5$ A^3/m^2. Other parameters used in this calculation include $\lambda(0K) = 100$ nm, $J_{\text{NL}}(T \to 0K) \simeq 6.5 \times 10^{12}$ A/m^2, $\lambda_{\text{cutoff}} = 800$ nm, $J_{\text{cutoff}} = 4.2 \times 10^{11}$ A/m^2, and $T_c = 34.6$ K with a standard deviation of Gaussian spread of $\delta T_c = 1.3$ K. The noise floor in the experiment is -143 dBm.

above the noise floor only in the high temperature region near T_c. The experimental data of the MgB_2 films from group A under a +18 dBm, 5.33 GHz microwave excitation is shown as blue dots. It is clear that this model predicts very low nonlinear response at low temperature. Hence, other mechanisms must be responsible for $P_{3f}(T)$ at temperatures below T_c.

V. NONLINEARITY DUE TO SECOND T_c WITH LEGGETT MODE AT LOW TEMPERATURE

Theoretically, the nonlinear response of a two-band superconductor should show a strong peak at the second T_c for completely decoupled bands [18]. With increasing interband coupling, the peak due to the second T_c will gradually shift to higher temperature and have a reduced peak value [18]. Therefore based on theory, it is possible that in addition to the nonlinearity coming from the first T_c, a proximity-enhanced second T_c also contributes to the intrinsic nonlinearity. From the $P_{3f}(T)$ data shown in Figs. 2 and 4, the second peak at 27 K (Fig. 2) or at 23 K (Fig. 4) may be due to this intrinsic mechanism. Another $P_{3f}(T)$ experiment was carried out with a loop probe which utilizes a smaller rf magnetic field and a large excitation area. The loop probe, providing an almost 1 mT in-plane magnetic field on the MgB_2 surface, is made of a nonmagnetic coaxial cable with its inner conductor (200 μm in diameter) forming a $\sim$500 μm outer-diameter semicircular loop shorted with the outer conductor [20]. This measurement is performed on the MgB_2 sample from group A and the loop probe is positioned on the same

region of the sample where the magnetic write head probe was placed. In order to compare to the result measured by the magnetic write head probe, both $P_{3f}(T)$ curves are lined up to -100 dBm at their peaks around 27 K, as shown in Fig. 9. The loop probe measurement shows only one peak at 27.8 K almost the same temperature as the second peak measured by the magnetic write head probe. The lack of a peak at the first T_c for the loop probe measurement is due to the weak magnetic field and therefore a small value of Γ in Eq. (2) at the highest T_c. The inset of Fig. 9 shows the power dependence of P_{3f} on P_f measured by the loop probe at the peak temperature. The slope of P_{3f} on P_f is 2.85, very close to 3, the theoretical value for the intrinsic nonlinear Meissner effect. However, the slope of P_{3f} on P_f obtained with the magnetic write head probe at this temperature is just 1.68. This implies that our magnetic write head probe excites another nonlinear mechanism in this temperature region and there is interference with the nonlinearity from the second T_c. The magnetic write head probe provides more intense and localized parallel magnetic fields on the superconductor sample surface. A comparison of magnetic fields generated by the magnetic write head probe and the loop probe are reported in Ref. [11]. It is unclear why the nonlinearity from the proximity-enhanced second T_c is more significant than that from the first T_c in the loop probe measurement.

Besides the intrinsic nonlinearity from the proximity-enhanced second T_c, an additional intrinsic nonlinearity arising from Josephson coupling between the σ and π bands would be expected [21] below the second peak at 27 K in Fig. 2 or at 23 K in Fig. 4. This nonlinear response

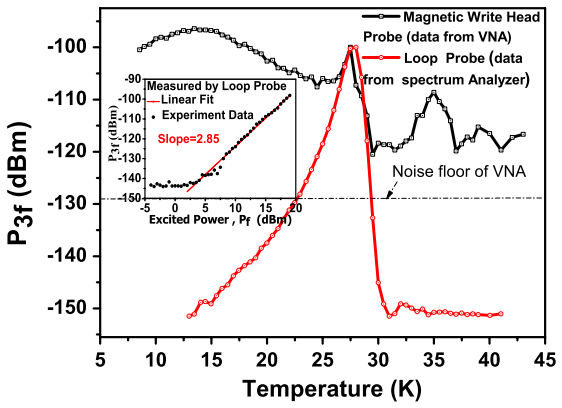

FIG. 9. Temperature dependence of P_{3f} from a 50 nm thick MgB_2 film (group A) measured by the loop probe (red curve) and magnetic write head probe (black curve), respectively. The excited frequency for both measurements is 5.33 GHz. The excited power is 20 and 14 dBm for loop probe and magnetic write head probe, respectively. Note that the VNA is used to perform the measurement with the write head probe and the spectrum analyzer is used in the measurement done by the loop probe. The VNA has higher noise floor ~ -130 dBm. The inset shows the P_{3f} vs P_f dependence for the loop probe measurement at 27.8 K.

(arising from the Leggett mode) comes from the variable phase difference of the superconducting order parameters in the two bands of MgB_2, and will only be excited when a nonequilibrium charge imbalance appears both at short length scales and at temperatures where the proximity-induced π band becomes superconducting [21]. In our magnetic write head experiment, the perpendicular component of the rf magnetic field results in a charge imbalance and excitation of the Leggett mode would be expected. From the experimental data of $P_{3f}(T)$ in Figs. 2 and 4, the nonlinearity below the second peak gradually increases with decreasing temperature before saturation. In this temperature regime, the nonlinearity could arise from the Leggett mode mechanism, although no calculation of this nonlinearity exists, to our knowledge. However, the observed temperature dependence of $P_{3f}(T)$ is reminiscent of that arising from Josephson weak links [22] or Josephson vortices in a large Josephson junction [20]. The absence of this signal in the macroscopic loop probe measurement is consistent with the charge imbalance mechanism.

VI. NONLINEARITY FROM THE REPORTED NODAL GAP SYMMETRY

Although MgB_2 is commonly believed to be a conventional s-wave superconductor, Agassi, Oates, and Moeckly claim that MgB_2 has line nodes in the superconducting gap, and they claim further that the gap has six nodes, as $\Delta(\phi, T) = \Delta_0(T) * \sin(6\phi)$ where ϕ is the azimuthal angle in the $\widehat{ab}$ plane of the hexagonal crystal, and $\Delta_0(T)$ is the weakly temperature-dependent amplitude of the gap function at low temperatures [8]. From their IMD measurement on MgB_2 films, the temperature-dependent $P_{\mathrm{IMD}}(T)$ shows an upturn around $T < 10$ K and increases as $1/T^2$ [9]. Therefore, based on these observations and proposals, we would also expect our measurement of $P_{3f}(T)$ to show an increase in the same temperature range. However, all of our experimental data show that $P_{3f}(T)$ tends to decrease at temperatures $T < 13$ K. If the prediction of the nodal gap symmetry is correct, the observed downturn may be due to the interference between the Leggett mode nonlinearity (or some other nonlinearity) and the nonlinearity from this nodal gap behavior. Another possibility may be that the rf magnetic fields employed in our experiment are too strong, or the temperatures are not sufficiently small to see the intrinsic NLME due to the nodes. Yet another possibility is the nonlinear response of the Andreev bound state, arising from a sign change of the superconducting gap, on the surface of MgB_2 [23,24]. Further investigation at lower temperature is required.

VII. NONLINEARITY FROM MOVING VORTICES

Vortex nucleation and penetration into the film induces a dynamic instability and generates harmonic response [25].

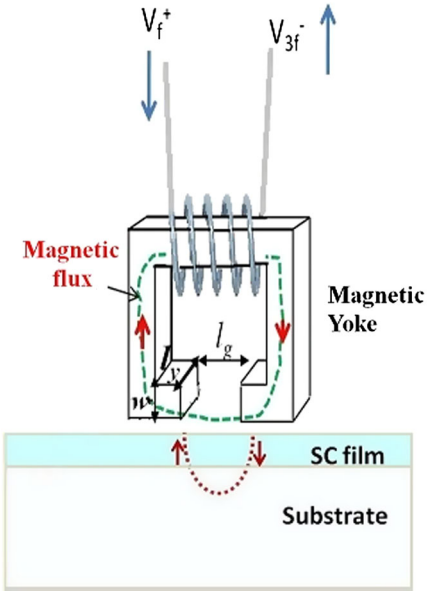

FIG. 10. Schematic illustration of the magnetic flux coming from the yoke of the magnetic write head to the superconductor (SC) where l_y, w, and l_g represent the width, the thickness, and the length of the gap, respectively. The length l_g is on the order of 100 nm for our write head probe. The width (l_y) is 200 nm and thickness (w) is around 1 μm. The figure is not to scale.

Considering the relation of the penetration depth of MgB_2 ($\sim$140 nm) and our film thickness (50 nm), the tendency to create a straight vortex parallel to the film surface will be suppressed. However, due to the magnetic field distribution from the magnetic write head probe, a significant vertical magnetic field is expected. Figure 10 shows a schematic illustration of our experiment in which the rf magnetic field from the magnetic write head probe interacts with the superconductor underneath the probe. A vortex and an antivortex nucleate perpendicular to the film and will move under the influence of the rf screening currents. One can model this situation with an equivalent point magnetic dipole that is placed above the superconducting thin film [26]. The creation, motion, and destruction of perpendicular vortex and antivortex pairs will generate high order harmonic response in the experiment. The nonlinear measurements in films from group A and group B would have nonlinearity from moving vortices in the entire temperature region under high rf magnetic field. In addition, vortex nonlinearity due to weak link coupling between each grain under the localized rf field may be another mechanism. The nonlinearity from weak link vortices in a YBCO bicrystal grain boundary has demonstrated a significant increasing nonlinearity with decreasing temperature following the temperature dependence of the critical current of the junction [20]. From the $P_{3f}(T)$ measurement of MgB_2 in Figs. 2 and 4, the trends of temperature-dependent nonlinearity below 30 K are very similar to the nonlinearity from the weak link vortices in a YBCO granular structure, except for the deep dip around 20 K in Fig. 4. Comparing the films of group A to that of group B, both Abrikosov vortex nonlinearity and weak link vortex nonlinearity of the films from group A would be expected to be more significant due to the exposure to air, which will degrade the film and therefore decrease the lower critical field of the weak links and grains. Models based on the creation and annihilation of perpendicular vortices and the weak link vortices are currently under development.

VIII. CONCLUSIONS

A strongly temperature-dependent third harmonic response is found from near field microwave microscopy measurement on high quality MgB_2 films. From the investigation of the third harmonic response as a function of temperature and input power level, the nonlinear mechanisms in high quality MgB_2 films appear to be quite complex. The nonlinear response near T_c can be well understood by a model relating modulation of the superconducting order parameter near T_c. However, the nonlinear response at temperature less than T_c shows several different possible nonlinear mechanisms. The first is the intrinsic nonlinearity from the proximity-induced second T_c. The second is the intrinsic nonlinearity arising from Josephson coupling between the σ and π bands. The third is the potential nonlinearity from the proposed nodal gap symmetry of MgB_2. Finally is the nonlinearity due to the perpendicular vortex pairs as well as the inevitable weak link vortices created in the high quality MgB_2 films by the high rf field probe.

ACKNOWLEDGMENTS

This work is supported by the U.S. Department of Energy/High Energy Physics through Grant No. DESC0004950, and also by the ONR AppEl, Task D10 (Award No. N000140911190), and CNAM. The work at Temple University is supported by DOE under Grant No. DE-SC0004410.

[1] J. Nagamatsu, Norimasa Nakagawa, Takahiro Muranaka, Yuji Zenitani, and Jun Akimitsu, Nature (London) **410**, 63 (2001).
[2] X. X. Xi, Supercond. Sci. Technol. **22**, 043011 (2009).
[3] R. L. Geng, G. V. Eremeev, H. Padamsee, and V. D. Shemelin, in *Proceedings of the 2007 Particle Accelerator Conference, Albuquerque, New Mexico* (IEEE, New York, 2007), p. 2337.
[4] T. Tajima, A. Canabal, Y. Zhao, A. Romanenko, B. H. Moeckly, C. D. Nantista, S. Tantawi, L. Phillips, Y. Iwashita, and I. E. Campisi, IEEE Trans. Appl. Supercond. **17**, 1330 (2007).
[5] A. Gurevich and G. Ciovati, Phys. Rev. B **77**, 104501 (2008).

[6] G. Cifariello, M. Aurino, E. D. Gennaro, G. Lamura, A. Andreone, P. Orgiani, and X. X. Xi, Appl. Phys. Lett. **88**, 142510 (2006).
[7] T. Dahm and D. J. Scalapino, Appl. Phys. Lett. **85**, 4436 (2004).
[8] Y. D. Agassi, D. E. Oates, and B. H. Moeckly, Phys. Rev. B **80**, 174522 (2009).
[9] D. E. Oates, Y. D. Agassi, and B. H. Moeckly, Supercond. Sci. Technol. **23**, 034011 (2010).
[10] D. E. Oates, S. H. Park, and G. Koren, Phys. Rev. Lett. **93**, 197001 (2004).
[11] Tamin Tai, X. X. Xi, C. G. Zhuang, D. I. Mircea, and S. M. Anlage, IEEE Trans. Appl. Supercond. **21**, 2615 (2011).
[12] X. Zeng, A. V. Pogrebnyakov, A. Kotcharov, J. E. Jones, X. X. Xi, E. M. Lysczek, J. M. Redwing, S. Y. Xu, J. Lettieri, D. G. Schlom, W. Tian, X. Q. Pan, and Z. K. Liu, Nat. Mater. **1**, 35 (2002).
[13] D. I. Mircea, H. Xu, and S. M. Anlage, Phys. Rev. B **80**, 144505 (2009).
[14] S. C. Lee, M. Sullivan, G. R. Ruchti, and S. M. Anlage, B. S. Palmer, B. Maiorov, and E. Osquiguil, Phys. Rev. B **71**, 014507 (2005).
[15] D. Agassi and D. E. Oates, Phys. Rev. B **72**, 014538 (2005).
[16] D. E. Oates, Y. D. Agassi, and B. H. Moeckly, IEEE Trans. Appl. Supercond. **17**, 2871 (2007).
[17] A. A. Gallitto, G. Bonsignore, and M. L. Vigni, Int. J. Mod. Phys. B **17**, 535 (2003).
[18] E. J. Nicol, J. P. Carbotte, and D. J. Scalapino, Phys. Rev. B **73**, 014521 (2006).
[19] S. X. Wang and A. M. Taratorin, *Magnetic Information Storage Technology* (Academic Press, San Diego, CA, 1999), Chap. 2, p. 38.
[20] S. C. Lee, S. Y. Lee, and S. M. Anlage, Phys. Rev. B **72**, 024527 (2005).
[21] A. Gurevich and V. M. Vinokur, Phys. Rev. Lett. **90**, 047004 (2003).
[22] C. Jeffries, Q. H. Lam, Y. Kim, L. C. Bourne, and A. Zettl, Phys. Rev. B **37**, 9840 (1988).
[23] A. Zare, T. Dahm, and N. Schopohl, Phys. Rev. Lett. **104**, 237001 (2010).
[24] A. P. Zhuravel, B. G. Ghamsari, C. Kurter, P. Jung, S. Remillard, J. Abrahams, A. V. Lukashenko, Alexey V. Ustinov, and Steven M. Anlage, arXiv:1208.1511.
[25] T. B. Samoilova, Supercond. Sci. Technol. **8**, 259 (1995).
[26] G. Carneiro, Phys. Rev. B **69**, 214504 (2004).